2019

Improving Performance of Inverse Compton Sources Through Laser Chirping

Balsa Terzić
Old Dominion University, bterzic@odu.edu

A. Brown
Old Dominion University

I. Drebot

T. Hagerman
Old Dominion University

E. Johnson
Old Dominion University

See next page for additional authors

Original Publication Citation

Terzić, B., Brown, A., Drebot, I., Hagerman, T., Johnson, E., Krafft, G. A., Maroli, C., Petrillo, V., & Ruijter, M. (2019). Improving performance of inverse Compton sources through laser chirping. *Europhysics Letters*, *126*(1), 1-7, Article 12003. https://doi.org/10.1209/0295-5075/126/12003

A Letters Journal Exploring the Frontiers of Physics

April 2019

EPL, **126** (2019) 12003 www.epljournal.org
doi: 10.1209/0295-5075/126/12003

Improving performance of inverse Compton sources through laser chirping

B. Terzić[1], A. Brown[1], I. Drebot[2], T. Hagerman[1], E. Johnson[1], G. A. Krafft[1,3], C. Maroli[2], V. Petrillo[2,4] and M. Ruijter[2,5]

[1] *Department of Physics, Center for Accelerator Science, Old Dominion University - Norfolk, VA 23529, USA*
[2] *INFN-Milan - via Celoria 16, 20133 Milano, Italy*
[3] *Thomas Jefferson National Accelerator Facility - Newport News, VA 23606, USA*
[4] *Università degli Studi di Milano - via Celoria 16, 20133 Milano, Italy*
[5] *Università di Roma La Sapienza - P.le A. Moro 5, 00185 Roma, Italy*

received 4 February 2019; accepted in final form 17 April 2019
published online 23 May 2019

PACS 29.20.Ej – Linear accelerators
PACS 29.25.Bx – Electron sources
PACS 07.85.Fv – X- and γ-ray sources, mirrors, gratings, and detectors

Abstract – We present a new method for computation of radiation spectra in the non-linear regime of operation of inverse Compton sources characterized by high laser intensities. The resulting simulations agree well with the experiments. Increasing the laser intensity changes the longitudinal velocity of the electrons during their collision, leading to considerable non-linear broadening in the scattered radiation spectra. The effects of such ponderomotive broadening are so deleterious that most inverse Compton sources either remain at low laser intensities or pay a steep price to operate at a small fraction of the physically possible peak spectral output. This ponderomotive broadening can be reduced by a suitable frequency modulation (also referred to as "chirping", which is not necessarily linear) of the incident laser pulse, thereby drastically increasing the peak spectral density. This frequency modulation, included in the new code as an optional functionality, is used in simulations to motivate the experimental implementation of this transformative technique.

Introduction. – When a relativistic electron beam interacts with a high-field laser beam, intense and highly collimated electromagnetic radiation will be generated through Compton scattering [1,2]. Through relativistic upshifting and the relativistic Doppler effect, highly energetic polarized photons are radiated along the electron beam motion when the electrons interact with the laser light. For example, x-ray radiation can be obtained when optical lasers are scattered from electrons of tens-of-MeV beam energy. Because of the desirable properties of the radiation produced, many groups around the world have been designing, building, and utilizing inverse Compton sources (ICS) for a wide variety of purposes. Sources of electromagnetic radiation relying upon Compton scattering are being applied in fundamental physics research, and compact accelerator-based sources specifically designed for potential user facilities have been built [3]. One remarkable feature of the radiation emerging from such sources, compared to bremsstrahlung sources, is its narrow-band nature. Applications to x-ray structure determination [4], dark-field imaging [5,6], phase contrast imaging [5], and computed tomography [7] have been demonstrated experimentally and take full advantage of the narrow bandwidth of ICS.

Depending on the properties of the two fundamental elements of ICS —the energy of an electron beam and the intensity of a laser— there are several regimes of operations, shown in fig. 1. With the increasing electron beam energies, there are: i) Thomson regime at low-to-medium electron beam energies ($2\gamma E_{\text{laser}} \ll m_e c^2$), where the electron recoil can be neglected; and ii) Compton regime at high electron beam energies ($2\gamma E_{\text{laser}} \sim m_e c^2$), requiring

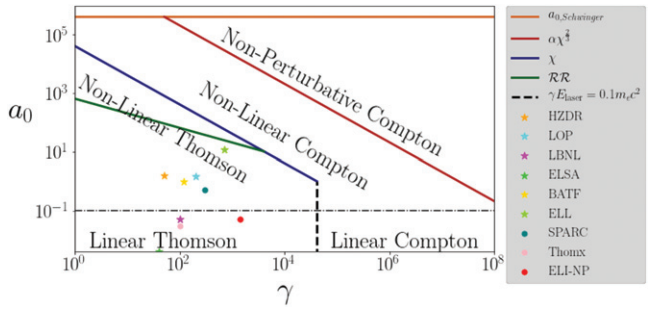

Fig. 1: Regimes of operation for ICS. The red line denotes the boundary between the non-perturbative and perturbative non-linear Compton regimes [8,9]. The blue line indicates the division between Thomson and perturbative Compton scattering. Between the blue and green lines the radiation reaction needs to be taken into account [10–12]. ICS that are in operation are marked as stars and future ICS as dots [13–19].

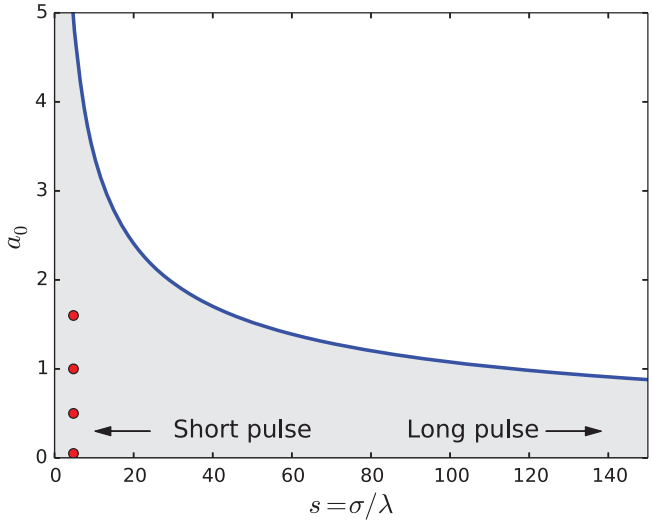

Fig. 2: Region of validity for SENSE shown in gray. Red dots denote the four experimental values for the laser field strength a_0 from the Dresden experiment [24].

proper accounting for electron recoil. As the laser intensity increases, there are: i) linear regime at low laser intensities; and ii) non-linear regime at high laser intensities. The onset of non-linearity is quantified by the increase in the amplitude of the normalized vector potential (a_0) representing the laser $\tilde{A}(\xi) = eA(\xi)/m_e c^2 = a(\xi)\cos(2\pi\xi/\lambda_0)$, where $a(\xi)$ is the laser envelope, $\xi = z + ct$ the coordinate along the laser pulse and λ_0 the mean wavelength of the laser.

In this letter, we develop a method for computation of radiation spectra emitted from ICS operating in the non-linear Thomson regime, extending to high laser intensities and low-to-medium electron beam energies. The resulting new computer code, SENSE (simulation of emitted non-linear scattering events), uses a three-dimensional (3D) pulse model for the laser beam, a significant generalization of the one-dimensional (1D) plane-wave model. The electron beam is either generated by randomly sampling its bulk properties or supplied as input.

SENSE code. – SENSE computes spectra of the scattered radiation in ICS by integrating a spectrum $\mathrm{d}^2E/\mathrm{d}\omega\mathrm{d}\Omega$ due to a collision of a single electron with a 3D laser pulse over an entire distribution of electrons. Monte Carlo integration over a solid angle $\mathrm{d}\Omega(\theta,\phi)$ of the physical aperture with the angular size of θ_a is used to compute a spectrum $\mathrm{d}E(\omega)/\mathrm{d}\omega = \int \mathrm{d}^2E(\omega;\Omega)/(\mathrm{d}\omega\mathrm{d}\Omega)\mathrm{d}\Omega$ for each of the N_s simulation particles sampling a distribution of N_e electrons. The total spectrum is the average of these individual spectra. It is written in Python, and uses Cython and `numpy` for computational efficiency [20,21]. It is parallelized to run on multiple CPUs.

SENSE is applicable in the non-linear Thomson regime, where electron recoil can be neglected [22]. The range of the laser field parameter a_0 for which this formalism is applicable is derived by requiring that the total number of photons emitted is less than one [23], and is given by $a_0 < \sqrt{3\lambda_0/(2\pi^{1/2}\alpha\sigma_{l,z})}$, with $\sigma_{l,z}$ the laser pulse length and α the fine structure constant. For the Dresden experiment [24] simulated in the next section $s = \sigma_{l,z}/\lambda_0 = 5.57$, so SENSE is applicable for the field strength parameter $a_0 < 4.56$. All simulations reported here are well within this limit, as are most other existing and future ICS. The parameter space for which SENSE is applicable is shown in fig. 2.

We compare our classical code SENSE to the quantum code CAIN [25] by carrying out simulations in the classical non-linear Thomson regime where electron recoil can be neglected. There is a fundamental difference between the Monte Carlo implementation in CAIN [25] and SENSE. Both codes start by randomly sampling the electron distribution. However, CAIN models the incoming laser beam scattering off each such electron from the sample with a number of individual scattered particles. While this directly models what happens in an experiment, albeit on orders-of-magnitude smaller scales, it ensures that the rare events in nature will be equally rare in a simulation, leading to poor statistics in those regions. In contrast, SENSE computes scattering probabilities —the likelihood of scattered photons to be found in each portion of the spectrum. Therefore, the accuracy in each portion of the spectrum computed by SENSE is the same, determined only by the accuracy of the Monte Carlo integration.

There are two important features of SENSE that CAIN either does not have or implements only in a cumbersome way: 1) an arbitrary shape of the laser pulse and 2) an arbitrary laser frequency modulation (FM) scheme.

SENSE uses the equations derived in [22] and amended for FM in [23] for backscattered, on-axis photons ($\phi = 0$, $\theta = 0$). It is first generalized to arbitrary angles ϕ and θ, in order to evaluate the total scattered radiation spectrum:

$$\frac{\mathrm{d}^2E}{\mathrm{d}\omega\mathrm{d}\Omega} = \frac{\mathrm{d}^2E_\sigma}{\mathrm{d}\omega\mathrm{d}\Omega} + \frac{\mathrm{d}^2E_\pi}{\mathrm{d}\omega\mathrm{d}\Omega}, \tag{1}$$

where

$$\frac{\mathrm{d}^2E_\sigma}{\mathrm{d}\omega\mathrm{d}\Omega} = \frac{e^2}{8\pi^2c^3}\omega^2\left|D_x\right|^2\sin^2\phi,$$
$$\frac{\mathrm{d}^2E_\pi}{\mathrm{d}\omega\mathrm{d}\Omega} = \frac{e^2}{8\pi^2c^3}\omega^2\left|D_x\left(\frac{\cos\theta-\beta_z}{1-\beta_z\cos\theta}\right)\cos\phi + D_z\sin\theta\right|^2, \tag{2}$$

$$D_{x,z} = c_{x,z}\int_{-\infty}^{\infty}\tilde{A}^{1,2}(\xi)\mathrm{d}\xi\exp\left[i\omega\left(\frac{\xi(1-\beta_z\cos\theta)}{c(1+\beta_z)}\right.\right.$$
$$-\frac{\sin\theta\cos\phi}{c\gamma(1+\beta_z)}\int_{-\infty}^{\xi}\tilde{A}(\xi')\mathrm{d}\xi'$$
$$\left.\left.+\frac{(1+\cos\theta)}{2c\gamma^2(1+\beta_z)^2}\int_{-\infty}^{\xi}\tilde{A}^2(\xi')\mathrm{d}\xi'\right)\right], \tag{3}$$

where $c_x = 1/(\gamma(1+\beta_z))$ and $c_z = 1/(\gamma^2(1+\beta_z)(1+\beta_z\cos\theta))$.

SENSE models electron beam's emittance and the energy spread with a geometric argument. The 3D pulsed nature of a laser is modeled by varying the effective field parameter for each electron based on its path through the laser.

An electron along the z-axis of collision passes through the laser pulse head on. An electron with transverse motion p_x, $p_y \neq 0$, will pass through the laser pulse at an angle, thereby extending its path by $1/r$:

$$r \equiv (p_z/\gamma)/\sqrt{p_x^2+p_y^2+(p_z/\gamma)^2} \leq 1. \tag{4}$$

Because each electron passing through a laser pulse see the same number of wavelengths, extending the path traveled means that the effective wavelength of the laser is increased $\lambda_0 = \bar{\lambda}_0/r$, or, equivalently, the frequency is decreased ("red-shifted") $\omega_0 = r\bar{\omega}_0$. The barred quantities are experimental parameters.

The resulting effects on scattered radiation frequency are obtained from $\omega = (1+\beta)^2\gamma^2\omega_0$. The effects of the energy spread can be found by replacing $\gamma \approx \bar{\gamma}\,(1+\Delta\gamma/\bar{\gamma})$ to obtain $\omega = \bar{\omega}r\,(1+2\Delta\gamma/\bar{\gamma}) \equiv k\bar{\omega}$, where $k \equiv r\,(1+2\Delta\gamma/\bar{\gamma})$. This means that in order to properly account for angles (emittance) and the energy spread, the computed spectra should be red-shifted by a factor $1/k$. Therefore, SENSE computes

$$\left(\frac{\mathrm{d}E(\omega)}{\mathrm{d}\omega}\right)_{\text{beam}} = \frac{N_e}{N_s}\sum_{i=1}^{N_s}\frac{\mathrm{d}E(\omega/k(x,y,p_x,p_y,\gamma))}{\mathrm{d}\omega}. \tag{5}$$

$\mathrm{d}E/\mathrm{d}\omega$ is computed by integrating $\mathrm{d}^2E/(\mathrm{d}\omega\mathrm{d}\Omega)$ over the physical aperture as shown in fig. 3.

In the 3D laser pulse model, the strength of the effective laser field that an electron experiences depends on its path. An on-axis electron "sees" the maximum strength.

We model electrons with angles as taking straight paths through the laser pulse. For an electron at the beginning of interaction with the laser beam ($t = 0$), the spatial

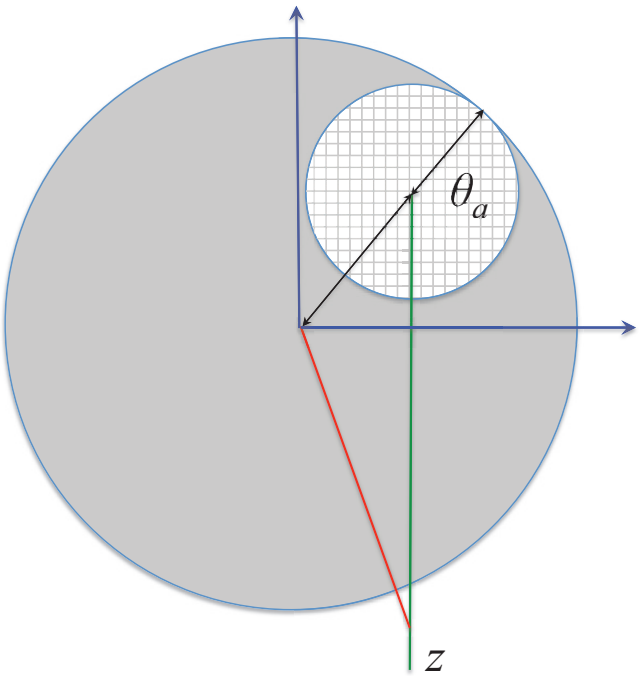

Fig. 3: Geometry of photon scattering. The checkered region represents the physical aperture θ_a. The shaded region is centered on the point where a scattered photon pierces the plane of the physical aperture. The green line is the z-axis. The red line denotes the path of a scattered photon. The polar coordinates $(\cos\theta, \phi)$ in which the integration is carried out are shown in blue.

coordinates are (x_0, y_0, z_0). The time coordinate is $t = (\xi - z_0)/c$. After normalizing transverse momenta $\tilde{p}_{x,y} \equiv p_{x,y}/(m_ec)$, an electron's trajectory is

$$x = x_0 + \tilde{p}_x\xi, \quad y = y_0 + \tilde{p}_y\xi, \quad z = z_0 + r\xi. \tag{6}$$

In these new coordinates, a Gaussian laser pulse with r.m.s size $\sigma_{x,l}$, $\sigma_{y,l}$, $\sigma_{z,l}$ as experienced by the electron is

$$a(\xi) = \tilde{a}_0\exp\left(-(\xi+\eta)^2/(2\tilde{\sigma}_{z,l}^2)\right), \tag{7}$$

where

$$\tilde{a}_0 = a_0\exp\left(-\frac{x_0^2}{2\sigma_{x,l}^2}-\frac{y_0^2}{2\sigma_{y,l}^2}-\frac{z_0^2}{2\sigma_{z,l}^2}\right)\exp\left(\frac{\eta^2}{2\tilde{\sigma}_{z,l}^2}\right),$$
$$\eta = \tilde{\sigma}_{z,l}^2\left(\frac{x_0\tilde{p}_x}{\sigma_{x,l}^2}+\frac{y_0\tilde{p}_{y,l}}{\sigma_{y,l}^2}+\frac{z_0r}{\sigma_{z,l}^2}\right),$$
$$\tilde{\sigma}_{z,l}^2 = \frac{\sigma_z^2}{r^2}\left(\frac{\tilde{p}_x^2\sigma_z^2}{r^2\sigma_{x,l}^2}+\frac{\tilde{p}_y^2\sigma_{z,l}^2}{r^2\sigma_{y,l}^2}+1\right)^{-1}.$$

The maximum magnitude of the vector potential a occurs at the center of the pulse, at $z_0 = 0$. This means that the new laser pulse shape given in eq. (7) is also a Gaussian, only with a changed size $\tilde{\sigma}_{z,l}$ and the amplitude of the normalized vector potential $\tilde{a}_0$. The change in the path

Table 1: Laser pulse and electron beam parameters from the Dresden experiment [24]. All σ quantities are reported as r.m.s.

Laser pulse				Electron beam			
Quantity	Variable	Value	Unit	Quantity	Variable	Value	Unit
Wavelength	λ_0	800	nm	Energy	E_e	23	MeV
Pulse duration	T	14.86	fs	Energy spread	$\Delta E_e/E_e$	0.00175	
Horizontal spot size	$\sigma_{x,l}$	13.59	μm	Horizontal spot size	σ_x	41 ± 1.2	μm
Vertical spot size	$\sigma_{y,l}$	13.59	μm	Vertical spot size	σ_y	81 ± 2	μm
Pulse length	$\sigma_{z,l} \equiv cT$	4.5	μm	Horizontal emittance (normalized)	$\epsilon_{x,n}$	20.3 ± 1.1	mm mrad
Normalized length	$s \equiv \sigma_{z,l}/\lambda_0$	5.57		Vertical emittance (normalized)	$\epsilon_{y,n}$	18.0 ± 6.6	mm mrad

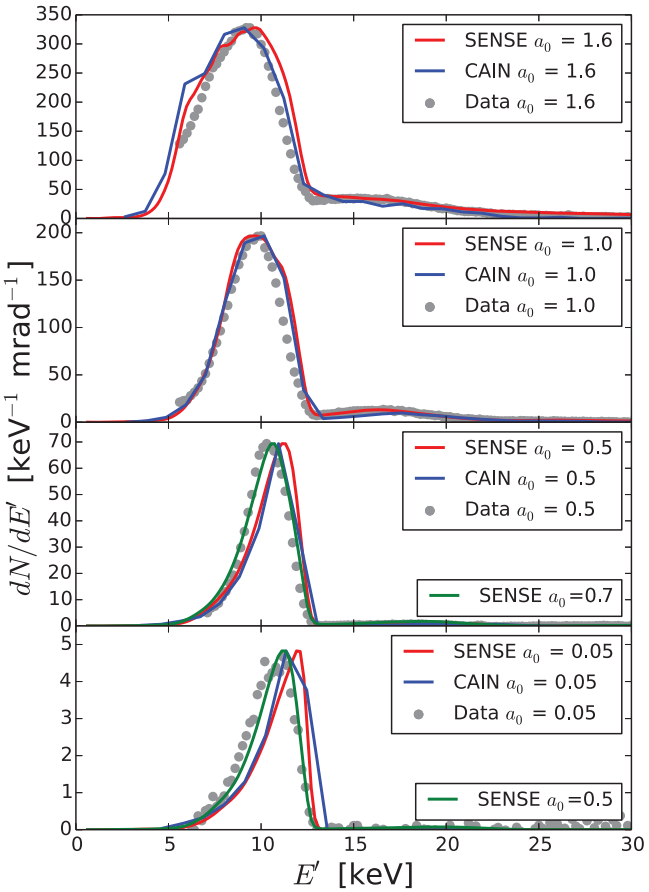

Fig. 4: Simulation of the Dresden experiment [24] data (gray circles) with CAIN (blue line) and with SENSE (red line) for parameters $a_0 = 1.6, 1.0, 0.5, 0.05$. Simulations with SENSE use $N_s = 4000$ particles and circular aperture of $\theta_a = 0.004$.

length of an electron's passage through the laser pulse is

$$\tilde{r} \equiv r\sqrt{\frac{\tilde{p}_x^2\sigma_{z,l}^2}{r^2\sigma_{x,l}^2} + \frac{\tilde{p}_y^2\sigma_{z,l}^2}{r^2\sigma_{y,l}^2} + 1}, \tag{8}$$

shifting the wavelength $\lambda_0 = \bar{\lambda}_0/\tilde{r}$. For electrons with angles $p_x, p_z \neq 0$, the ratio $\tilde{r}$ can be smaller (larger) than unity, in which case the frequencies are red-(blue-)shifted.

Simulating experimental results. – We simulate the Dresden experiment [24] using both CAIN [25] and SENSE. We assume that both the laser pulse and the electron beam are Gaussian-distributed with r.m.s sizes as reported in table 1 [24]. At the collision, the centers of the two beams overlap. The simulations with both CAIN and SENSE seem to be insensitive to the size and shape of the aperture. The aperture used in SENSE simulation is circular, while the physical aperture used in the Dresden experiment was rectangular [24]. In all of our simulations —those reported here and many others— the agreement between the results produced by CAIN and SENSE is remarkable, especially considering that they are based on two vastly different approaches.

The simulations in fig. 4 model the results of fig. 3 from ref. [24]. For the largest values of the laser field, $a_0 = 1.6, 1.0$, the agreement between the experiments and simulations using CAIN is very good, and SENSE even better. However, for lower values, $a_0 = 0.5, 0.05$, there is a shift to the right in the simulations from both codes. Increasing the strength of the laser field from $a_0 = 0.5$ to 0.7 and from $a_0 = 0.05$ to 0.5 in SENSE simulation produces excellent fits to the data, comparable to those for the larger values of a_0. The discrepancy between the experiments and the simulations for the lower values of the strength of the laser field is likely due to a different geometry of collision. It is unclear which of the geometries reported in fig. 2 of ref. [24] was used in experiments.

Improved performance via laser chirping. – In this section, we first discuss in general how chirping the laser pulse improves the peak spectral density in scattered radiation. We then use SENSE to simulate what would happen if the laser pulse in the Dresden experiment were chirped.

In ref. [23], we presented a novel and quite general analysis of the interaction of a high-field FM (chirped) 1D plane-wave laser and a relativistic electron, in which exquisite control of the spectral brilliance of the up-shifted Compton scattered photon is shown to be possible. The main idea behind laser chirping is the following: in order to minimize the spectral width in the lab frame, one should arrange the frequency in the beam frame to emit radiation Doppler shifted back to a constant frequency in the lab frame. This results in the judicious modulation of the frequency of the incoming laser pulse. We showed that the ponderomotive broadening can be eliminated by suitable FM of the incident laser. We suggested a practical realization of this compensation idea in terms of a chirped-beam–driven free electron laser oscillator and showed that signifi-

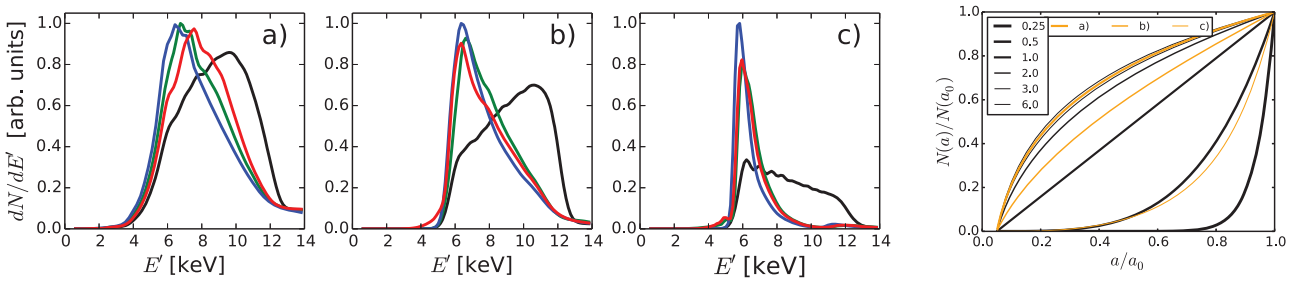

Fig. 5: Panels (a)–(c): simulation of the Dresden experiment [24] for $a_0 = 1.6$ using SENSE without FM (black lines) and with FM: optimal 1D plane-wave f_{1D} [23] (blue lines), optimal 3D laser pulse f_{3D} [26] (green lines) and RF FM [23] f_{RF} (red lines). The transverse electron beam size is nominal in (a), reduced by $\sqrt{10}$ in (b) and reduced by 10 in (c). Far right: distribution of field strength values a seen by the electron beam for various transverse ratios ($r_x = r_y = 0.25, 0.5, 1, 2, 3, 6$) in black. Shown in orange are the distributions corresponding to panel (a) with $r_x = 3$, $r_y = 6$, panel (b) with $r_x = 1$, $r_y = 2$, and panel (c) with $r_x = 0.3$, $r_y = 0.6$. A lower cutoff of $a > a_{\min} = 0.05$ is imposed on the distribution.

cant compensation can occur, even with the imperfect matching.

Extending the FM technique from the 1D plane-wave to the 3D pulse model for the laser has been carried out recently [26]. Because the electrons colliding with a 3D laser pulse encounter a full range of laser field strengths a, from 0 to a_0 —depending on which portion of the pulse they pass through— the a-dependent FM of the laser pulse cannot recover the narrow bandwidth of every electron in the distribution. Here we try to answer by how much the peak spectral density can be increased by a FM of the laser pulse and when FM is most effective.

SENSE is capable of simulating FM of any form. The FM laser pulse is represented by a normalized vector potential $\tilde{A}(\xi) = a(\xi)\cos(2\pi\xi f(\xi)/\lambda_0)$, where $f(\xi)$ is the FM prescription. We carried out simulations for a Gaussian laser pulse with three FM prescriptions $f(\xi)$:

1) Optimal chirping for the 3D laser pulse model [26]:

$$f_{3D}(Y;p) = f_0\left(\frac{p}{3} + \frac{1}{Y}\int_0^Y \mathrm{d}Y'(s_1'(Y') + s_2'(Y'))\right), \tag{9}$$

where $A(Y) = a_0\exp\left(-2Y^2\right)/2$, $Y = \xi/(\sqrt{2}\sigma)$, and p is an arbitrary constant and

$$s_{1,2} = \left[\frac{p}{2}A(Y) + \frac{p^3}{27} \pm \sqrt{\frac{p^4}{27}A(Y) + \frac{p^2}{4}A^2(Y)}\right]^{1/3}. \tag{10}$$

2) Optimal chirping for the 1D plane-wave model [23]:

$$f_{1D}(\xi;a) = f_0\left(1 + \frac{\sqrt{\pi}\sigma a^2}{4\xi}\mathrm{erf}(\xi/\sigma)\right), \tag{11}$$

with a the laser field strength, which varies from 0 to the maximum field strength a_0.

3) FM produced by a free electron laser oscillator. When a driving beam bunch is long enough that the radio frequency (RF)-curvature–related energy spread is substantial, the frequency of the laser pulse produced will also be modulated [23]:

$$f_{RF}(\xi;\lambda_{RF}) \approx f_0\left(\frac{1}{2} + \frac{\lambda_{RF}}{8\pi\xi}\sin\left(4\pi\xi/\lambda_{RF}\right)\right), \tag{12}$$

where λ_{RF} is the RF wavelength [23].

f_0 is a normalization constant such that $f_0\omega_0$ is the laser frequency at the center of the pulse. The normalization constant f_0 shifts the scattered energy spectrum by a factor f_0, without changing its shape. In the original derivation of the optimal FM for a 1D plane wave [23], $f_0 = 1/(1+a_0^2/2)$ was adopted, such that $f_{1D}(0) = 1$, while consequent studies used f_0 such that $f(\pm\infty) = 1$ [27,28]. In the original derivation of the optimal FM for a 3D laser pulse [26], f_0 such that $f(\pm\infty) = 1$ was applied. In the simulations reported here, f_0 was chosen to make $f(0) = 1$ for all three FMs: numerically computed for f_{3D}, $f_0 = 1/(1 + a_0^2/2)$ for f_{1D} and $f_0 = 2/3$ for f_{RF}.

All three FMs are one-parameter functions. The peak spectral density is maximized by carrying out a systematic search over their respective parameters using a genetic algorithm [23,29].

The distribution of the laser field strength a that a Gaussian-distributed electron beam "sees" as it passes through the center of a Gaussian laser pulse is quantified by a cumulative distribution

$$\frac{N(a)}{N(a_0)} = 1 - \frac{4}{\pi}\int_0^{h(a)}\mathrm{d}y\int_0^{g(a,y)}\mathrm{d}x\ \exp\left(-x^2 - y^2\right), \tag{13}$$

where $g(a,y) = \sqrt{\left[\log\left(a/a_0\right) + r_y^2y^2\right]/r_x^2}$, $h(a) = \sqrt{-\log\left(a/a_0\right)/r_y^2}$. $r_x \equiv \sigma_x/\sigma_{x,l}$, $r_y \equiv \sigma_y/\sigma_{y,l}$ are the ratios of transverse sizes of the two beams. Typical distributions are shown in the rightmost panel of fig. 5.

The smaller the ratios r_x, r_y, the larger the transverse size of the laser pulse in comparison to that of the electron beam, and the more peaked the distribution $N(a)/N(a_0)$ around $a = a_0$. Vanishing ratios r_x, r_y lead to the 1D

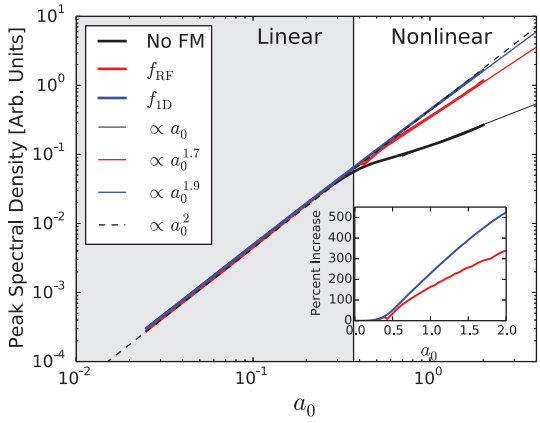

Fig. 6: The peak spectral density of back-scattered radiation for an on-axis electron passing through the laser as in the Dresden experiment [24], as a function of the laser field strength a_0, with 1D FM (red lines), RF FM (blue lines) and without FM (black lines). This is a 1D plane-wave limit in which FM is most effective. The inset shows the percent increase due to chirping.

plane-wave model in which all electrons experience the same strength of the laser field $a = a_0$. The closer the beam sizes are to this 1D plane-wave limit, the more effective the FM is. This is shown in fig. 5.

Reducing the transverse size of the electron beam relative to the laser pulse —approaching the 1D plane-wave approximation in which most electrons "see" a laser field whose strength is narrowly distributed near the maximum value of a_0— makes FM more efficient in increasing the peak spectral density of the scattered radiation. The increase due to FM depends on the relative sizes of the two beams, and can easily exceed 100% for electron beams that are half the transverse size of the laser pulse or smaller. It is also more pronounced at a larger value of the laser field strength, as can be seen in fig. 6. The scattered energy at which the peak spectral density occurs can be controlled by the normalization constant f_0 of the FM which only shifts the spectrum and does not change its shape. For the electron beams that are transversally small when compared to the laser pulse, when FM is most effective, the peak of the spectrum will be located just beyond $4f_0\gamma^2 E_{\rm laser}/(1 + a_0^2/2)$.

The increase of the peak spectral density for the laser pulse without FM exhibits quadratic dependence on the laser field strength a_0 in the linear regime, but only linear in the non-linear regime (fig. 6). All three FMs allow the dependence of the peak spectral density on the laser field to remain nearly quadratic throughout the non-linear regime, thereby substantially improving the return on investment in increasing laser intensity.

After comparing the efficiency of the three FM functional forms —optimal 3D laser pulse f_{3D} [26], optimal 1D plane-wave f_{1D} [23] and the RF-induced f_{RF} [23]— we find that they all are within about 20% of each other, with f_{1D} performing best. f_{RF} FM, the only form of the three attainable in the lab, can lead to a substantial increase in the peak spectral density —exceeding a factor of two for small electron beams at large strengths of the laser field parameter. This FM should be used in any future experiments involving laser chirping.

Conclusion. – Our new code SENSE is in excellent agreement with the established code CAIN, and over which it offers several crucial advantages: i) superior accuracy; ii) better efficiency in cases marred by poor statistics; iii) arbitrary shape of the laser pulse; and iv) ability to model an arbitrary FM.

The exceptional level of accuracy of SENSE allows us to combine it with a multidimensional non-linear optimization tool, such as a genetic algorithm, and use it as both a diagnostic and an optimization tool. The set of parameter values (emittance and the energy spread of the electron beam; size of the laser pulse and possibly others) which minimizes the r.m.s difference between the experiment and simulations pinpoints their actual experimental values. Similarly, this optimization tool can be used to find a set of parameter values which maximize the peak spectral density or minimize the radiation bandwidth, thereby improving the performance of the ICS.

The remarkable agreement between experiments and our new code SENSE strongly suggests that the underlying model correctly captures the relevant physics. This translates into confidence that SENSE can accurately describe physical behavior of collisions between electron beams and chirped laser pulses, a scenario which is yet to be tested experimentally. Simulations with SENSE strongly suggest that judiciously chirping the laser pulse substantially increases the spectral density. The increase depends on the strength of the laser field, the relative transverse sizes of the two beams and the form of the FM function. While for the current parameters in the Dresden experiment the returns due to chirping would be modest ($\approx 20\%$ for $a_0 = 1.6$), reducing the transverse size of the electron beam by a factor of ten should yield a threefold increase in the peak spectral density.

* * *

We are grateful to Mohammed Zubair for his insight and consultation into computational methods. This paper is authored by Jefferson Science Associates, LLC under U.S. DOE Contract No. DE-AC05-06OR23177. BT acknowledges the support from the U.S. National Science Foundation award No. 1535641.

REFERENCES

[1] Jackson J. D., *Classical Electrodynamics* (Wiley) 2007.
[2] Krafft G. A. and Priebe G., *Rev. Accel. Sci. Technol.*, **03** (2010) 147.
[3] Huang Z. and Ruth R. D., *Phys. Rev. Lett.*, **80** (1998) 976.

[4] Abendroth J., McCormick M. S., Edwards T. E., Staker B., Loewen R., Gifford M., Rifkin J., Mayer C., Guo W., Zhang Y., Myler P., Kelley A., Analau E., Hewitt S. N., Napuli A. J., Kuhn P., Ruth R. D. and Stewart L. J., *Phys. Rev. Accel. Beams*, **11** (2010) 91.
[5] Bech M., Bunk O., David C., Ruth R., Rifkin J., Loewen R., Feidenhans'l R. and Pfeiffer F., *J. Synchrotron Radiat.*, **16** (2009) 43.
[6] Schleede S., Meinel F. G., Bech M., Herzen J., Achterhold K., Potdevin G., Malecki A., Adam-Neumair S., Thieme S. F., Bamberg F., Nikolaou Ko., Bohla A., Yildirim A. Ö., Loewen R., Gifford M., Ruth R., Eickelberg O., Reiser M. and Pfeiffer F., *Proc. Natl. Acad. Sci. U.S.A.*, **109** (2012) 17880.
[7] Achterhold K., Bech M., Schleede S., Potdevin G., Ruth R., Loewen R. and Pfeiffer F., *Sci. Rep.*, **3** (2013) 1313.
[8] Nikishov A. I. and Ritus V. I., *J. Exp. Theor. Phys.*, **19** (1964) 529.
[9] Fedotov A., *J. Phys.: Conf. Ser.*, **826** (2017) 012027.
[10] Di Piazza A., *Lett. Math. Phys.*, **83** (2008) 305.
[11] Hadad Y., Labun L., Rafelski J., Elkina N., Klier C. and Ruhl H., *Phys. Rev. D*, **82** (2010) 096012.
[12] Ruijter M., Kharin V. Y. and Rykovanov S. G., *J. Phys. B: At. Mol. Opt. Phys.*, **51** (2018) 225701.
[13] Schramm U. *et al.*, *J. Phys.: Conf. Ser.*, **874** (2017) 012028.
[14] Phuoc K., Corde S., Thaury C., Malka V., Tafzi A., Goddet J. P., Shah R. C., Sebban S. and Rousse A., *Nat. Photon.*, **6** (2012) 308.
[15] Pogorelsky I. V., Ben-Zvi I., Hirose T., Kashiwagi S., Yakimenko V., Kusche K., Siddons P., Skaritka J., Kumita T., Tsunemi A., Omori T., Urakawa J., Washio M., Yokoya K., Okugi T., Liu Y., He P. and Cline D., *Phys. Rev. ST Accel. Beams*, **3** (2000) 090702.
[16] Schoenlein R. W., Leemans W. P., Chin A. H., Volfbeyn P., Glover T. E., Balling P., Zolotorev M., Kim K.-J., Chattopadhyay S. and Shank C. V., *Science*, **274** (1996) 236.
[17] Chauchat A. S., Le Flanchec V., Binet A., Flament J. L., Balleyguier P., Brasile J. P., Muller S. and Ortega J. M., *Nucl. Instrum. Methods Phys. Res. Sect. A*, **608** (2009) S99.
[18] C. Vaccarezza *et al.*, in *Proceedings of the 2014 International Particle Accelerator Conference, Dresden, Germany* (Curran Associates, Inc., Red Hook, New York) 2014, p. 267.
[19] Bruni C., Chiche R., Cizeron R., Fedala Y., Haissinski J. *et al.*, `http://hal.in2p3.fr/in2p3-00448278` (2010).
[20] The Python programming language, `http://www.python.org`.
[21] Cython: C-extensions for Python, `http://www.cython.org`.
[22] Krafft G. A., *Phys. Rev. Lett.*, **92** (2004) 204802.
[23] Terzić B., Deitrick K., Hofler A. S. and Krafft G. A., *Phys. Rev. Lett.*, **112** (2014) 074801.
[24] Krämer J. M., Jochmann A., Budde M., Bussmann M., Couperus J. P., Cowan T. E., Debus A., Köhler A., Kuntzsch M., Laso García A., Lehnert U., Michel P., Pausch R., Zarini O., Schramm U. and Irman A., *Sci. Rep.*, **8** (2018) 1398.
[25] Chen P., Horton-Smith G., Ohgaki T., Weidemann A. W. and Yokoya K., *Nucl. Instrum. Methods Phys. Res. Sect. A*, **355** (1995) 107.
[26] Maroli C., Petrillo V., Drebot I., Serafini L., Terzić B. and Krafft G. A., *J. Appl. Phys.*, **124** (2018) 063105.
[27] Rykovanov S. G., Geddes C. G. R., Schroeder C. B., Esarey E. and Leemans W. P., *Phys. Rev. Accel. Beams*, **19** (2016) 030701.
[28] Terzić B. and Krafft G. A., *Phys. Rev. Accel. Beams*, **19** (2016) 098001.
[29] Hofler A., Terzić B., Kramer M., Zvezdin A., Morozov V., Roblin Y., Lin F. and Jarvis C., *Phys. Rev. ST Accel. Beams*, **16** (2013) 010101.